ARTICLE

Nanodisco Balls: Control over Surface *versus* Core Loading of Diagnostically Active Nanocrystals into Polymer Nanoparticles

Peter Chhour,[†,‡] Nicolas Gallo,[†] Rabee Cheheltani,[†] Dewight Williams,[§] Ajlan Al-Zaki,[‡] Taejong Paik,[∥] Jessica L. Nichol,[⊗] Zhicheng Tian,[⊗] Pratap C. Naha,[†] Walter R. Witschey,[†] Harry R. Allcock,[⊗] Christopher B. Murray,[∥,#] Andrew Tsourkas,[†] and David P. Cormode[*,†,‡,⊥]

[†]Departments of Radiology, [‡]Bioengineering, [§]Biochemistry and Biophysics, [⊥]Cardiology, [∥]Chemistry, and [#]Materials Science and Engineering, University of Pennsylvania, 3400 Spruce Street, 1 Silverstein, Philadelphia, Pennsylvania 19104, United States and [⊗]Department of Chemistry, Pennsylvania State University, University Park, Pennsylvania 16802, United States

ABSTRACT Nanoparticles of complex architectures can have unique properties. Self-assembly of spherical nanocrystals is a high yielding route to such systems. In this study, we report the self-assembly of a polymer and nanocrystals into aggregates, where the location of the nanocrystals can be controlled to be either at the surface or in the core. These nanospheres, when surface decorated with nanocrystals, resemble disco balls, thus the term nanodisco balls. We studied the mechanism of this surface loading phenomenon and found it to be Ca^{2+} dependent. We also investigated whether excess phospholipids could prevent nanocrystal adherence. We found surface loading to occur with a variety of nanocrystal types including iron oxide nanoparticles, quantum dots, and nanophosphors, as well as sizes (10−30 nm) and shapes. Additionally, surface loading occurred over a range of polymer molecular weights (∼30−3000 kDa) and phospholipid carbon tail length. We also show that nanocrystals remain diagnostically active after loading onto the polymer nanospheres, *i.e.*, providing contrast in the case of magnetic resonance imaging for iron oxide nanoparticles and fluorescence for quantum dots. Last, we demonstrated that a fluorescently labeled protein model drug can be delivered by surface loaded nanospheres. We present a platform for contrast media delivery, with the unusual feature that the payload can be controllably localized to the core or the surface.

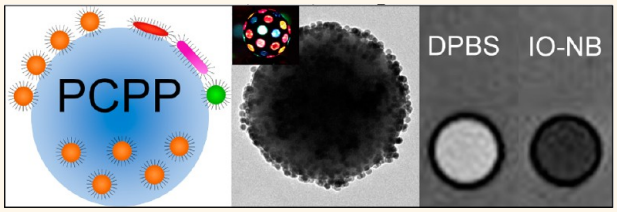

KEYWORDS: directed assembly · nanoparticles · polyphosphazene · MRI · multimodal · theranostic

Methods to create complex nanoparticle architectures such as stars, shells, cubes, and frames have led to structures with unique properties.[1−4] However, direct syntheses of such structures are frequently low yielding and difficult to scale up. An alternative approach is to form complex architectures from self-assembly of simpler, high-yielding components. One such route is incorporation of inorganic nanocrystals into polymeric nanoparticles. Such assemblies have a wide range of applications including uses in catalysis,[5] energy,[6] drug delivery,[7,8] and medical imaging.[9] Often, the structural organization of these nanoparticles will dictate its function and behavior in a given application. For example, previous research has shown that gold nanoparticles are capable of quenching the emission of nearby fluorescent sources when closely arranged. Jennings *et al.* showed that fluorescence could be recovered by separating the 1.5 nm gold nanoparticles and fluorophore a distance as little as 15 nm.[10] Hence, separate core and surface loading of gold cores and fluorophores could maintain fluorophore fluorescence. Therefore, the ability to control localization of nanocrystals *via* self-assembly would be a valuable tool in the synthesis of nanocrystal/polymer composite particles. Control over nanocrystal distribution within the core of polymer constructs has previously been demonstrated.[11−17] For instance, Luo *et al.* found that by modifying the surface ligands of

* Address correspondence to david.cormode@uphs.upenn.edu.

Received for review May 19, 2014 and accepted September 4, 2014.

Published online September 04, 2014
10.1021/nn502730q

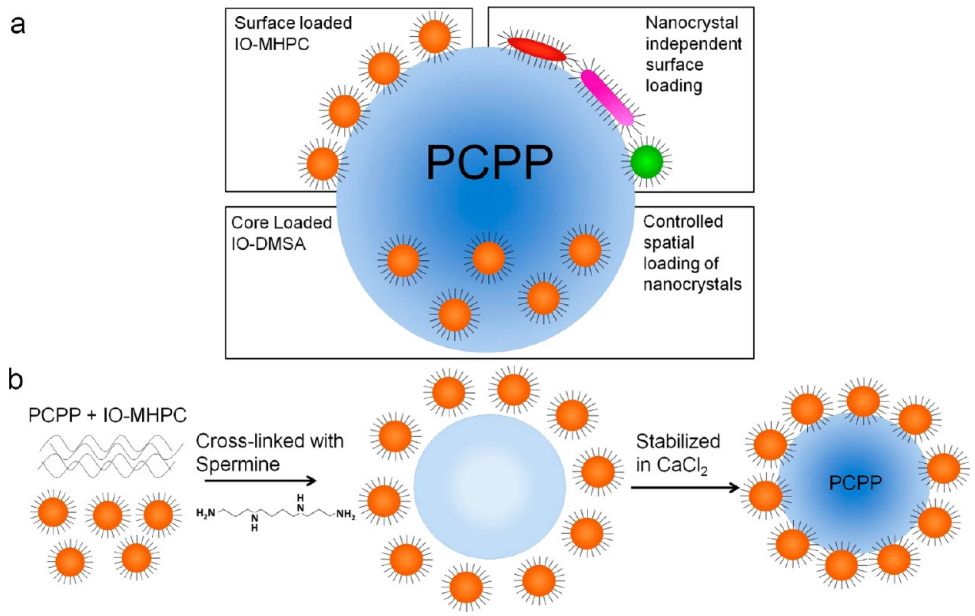

Figure 1. (a) Schematic overview of PCPP nanosphere platform. (b) Schematic of PCPP nanosphere synthesis.

gold nanoparticles, their incorporation could be focused to specific regions (*i.e.*, the core center or at the edge of the core) within nanoparticles formed from amphiphilic copolymers of polystyrene and poly(acrylic acid).[18]

In this study, we report the serendipitous discovery of a system where nanocrystals can be selectively loaded onto the *surface* of polymer nanospheres, as opposed to the core. This forms a structure reminiscent of a disco ball, which we term a nanodisco ball. We have found that phospholipid coated inorganic nanoparticles can be used to surface decorate a polymer nanosphere formed from poly(bis(4-carboxyphenoxy)phosphazene), or PCPP, whereas carboxylic acid coated nanocrystals localize to the core. PCPP is a part of a larger class of phosphorus−nitrogen backbone based polymers called polyphosphazenes.[19] These polymers have drawn interest for use in biomedical applications due to their tunable functionality and biocompatibility.[20−22] By modifying the polyphosphazene side chains and molecular weight, the biodegradation rate of polymers can be controlled, making this a promising platform for drug and contrast agent delivery.[23,24] Specifically, PCPP has been used to form ionically cross-linked hydrogels,[25,26] polymer films,[27] and more recently microencapsulating spheres.[23,28,29] This is the first report of a system that integrates polyphosphazenes and nanocrystals. Furthermore, this is a rare instance of a system where nanocrystals can be preferentially loaded onto the surface of a particle as opposed to internal loading. We believe that this novel system has excellent potential as a contrast agent or theranostic delivery platform.

Herein, we investigate the conditions for surface localization of nanocrystals onto PCPP nanospheres

TABLE 1. Definitions for Abbreviations Used

abbreviation	definition
PCPP	poly(bis(4-carboxyphenoxy)phosphazene)
MHPC	1-myristoyl-2-hydroxy-*sn*-glycero-3-phosphocholine
IONP	oleic acid coated iron oxide nanoparticles
IO−DMSA	dimercaptosuccinic acid coated iron oxide nanoparticles
IO-MHPC	MHPC micelle encapsulated iron oxide nanoparticles
IO-NB	PCPP nanospheres surface loaded with IO-MHPC
IO-DMSA-PCPP	PCPP nanospheres core loaded with IO-DMSA
FITC-BSA	bovine serum albumin conjugated with fluorescein isothiocyanate
FITC-PCPP	FITC-BSA loaded PCPP nanospheres
FITC-NB	FITC-BSA loaded IO-NB

(Figure 1a,b, Table 1). We report the synthesis of these nanodisco balls and their characterization *via* transmission electron microscopy, scanning electron microscopy, and electron microscopy tomography. They can be loaded with separate core and surface payloads, maximizing contrast for two imaging methods. We have probed the synthetic process for the key steps in the formation of the nanodisco balls. We evaluated the effects of varying the physical and chemical properties of the nanocrystals used on surface loading. We also varied phospholipid tail length for micelle formation and PCPP molecular weights for synthesis. In addition, we have investigated how competing micelles might affect the adherence of nanocrystals. Lastly, we assessed the diagnostic, drug delivery, and biological application of nanodisco balls.

RESULTS

Surface Decoration of PCPP Nanospheres. PCPP is a biocompatible polymer, which we have used to create a novel platform to exploit for nanocrystal delivery

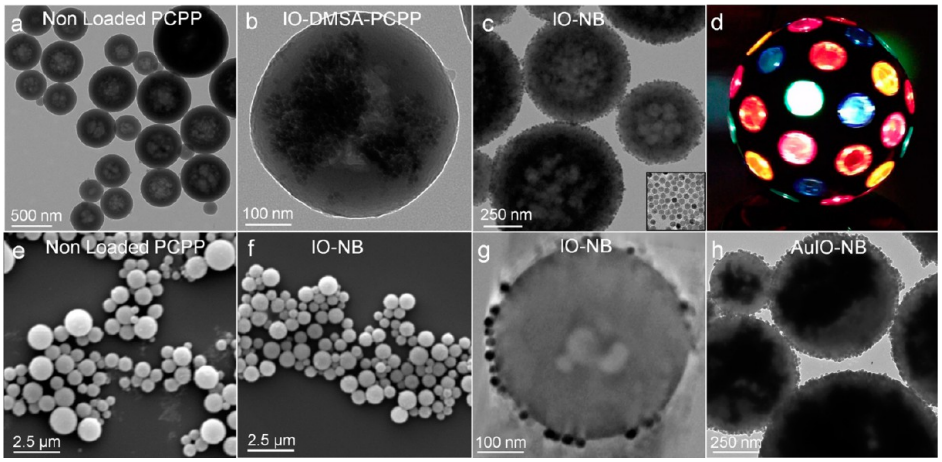

Figure 2. Electron microscopy images of PCPP nanospheres. TEM images of (a) nonloaded PCPP nanospheres, (b) IO-DMSA core loaded into PCPP nanospheres, (c) IO-MHPC surface loaded PCPP nanospheres (IO-NB). (d) Image of disco ball. SEM images of (e) nonloaded PCPP and (f) IO-NB. (g) *z*-slice of tomographic reconstruction of IO-NB. (h) Localization control of IO-MHPC and AuNP with PCPP nanospheres.

in biomedical applications. PCPP nanospheres were synthesized using a modified method that was previously developed to make microspheres.[28] The polycarboxylate PCPP is cross-linked with the polycation spermine to form polymer spheres. The self-assembled nanospheres were dispersed in $CaCl_2$, which we found necessary to halt nanoparticle growth.[30] This process resulted in polymer nanoparticles of 508 ± 185 nm (Figure 2a). As an initial step in loading these polymer nanoparticles, we added dimercaptosuccinic acid coated iron oxides (IO-DMSA) to the synthesis prior to adding the spermine cross-linker. We found that IO-DMSA were included in the core of the polymer spheres (Figure 2b). We then decided to explore the incorporation of iron oxide nanoparticles with alternative coatings.

Lipid coatings are commonly used to make nanocrystals biocompatible.[31] Oleic acid coated nanocrystals were rendered water-soluble through encapsulation in micelles formed by MHPC.[32,33] We mixed these phospholipid coated nanocrystals with PCPP before the addition of spermine. In the final product, we found that, surprisingly, the nanocrystals were exclusively localized to the surface of the nanospheres in a structure we found reminiscent of a disco ball (Figure 2c,d, supporting movie 1, Supporting Information). Electron microscopy images of these IO-MHPC surface loaded PCPP nanoparticles, or iron oxide loaded nanodisco balls (IO-NB), can be seen in Figure 2c. The average diameter of IO-NB was found to be 384 ± 127 nm (from analysis of 100+ nanoparticles in TEM images). SEM images revealed IO-NB to be an average diameter of 473.7 ± 125.9 nm and nonloaded PCPP nanospheres to be 548.7 ± 200.8 nm. (Figure 2e,f). Three dimensional tomographic reconstructions were performed to confirm the localization of IO-MHPC within PCPP nanoparticles. The reconstructions proved exclusive loading of IO-MHPC on the surface of PCPP nanospheres (Figure 2g). The total surface area available for IO- MHPC binding was calculated using the average size of PCPP nanospheres and found to be 123.2 cm^2/mg polymer. The total occupied binding space of IO-MHPC was found to be 96.96 cm^2, *i.e.*, 78.7%. This coverage corresponds to 609 IO-MHPC particles per PCPP nanosphere. However, we found that the coating density could be tuned, depending on the amount of IO-MHPC added in the synthesis procedure. These calculations can be found in the Supporting Information.

Next, we studied whether two types of nanocrystal could be loaded into the PCPP nanoparticles. We added both carboxylic acid coated gold nanoparticles and IO-MHPC to the synthesis at the same time. As can be seen in Figure 2h and supporting movies 2 and 3 (Supporting Information), the gold nanoparticles could be selectively localized to the core, while the IO-MHPC were localized to the particle surface (in supporting movie 2, low iron oxide and gold loading was used for clarity. However, much higher gold loading is possible, see Figure S1, Supporting Information). Gold nanoparticles produce computed tomography (CT) contrast in high concentrations, with no access to water needed;[34,35] therefore, core loading is best for gold nanoparticles. On the other hand, less iron oxide is needed to produce MRI contrast and access to water is needed, which surface loading provides. This formulation demonstrates the benefits of selective nanocrystal localization *via* optimization of the contrast properties for each technique.

Having made the surprising observation of surface loading of PCPP nanospheres with IO-MHPC, we probed the role of different steps in the synthesis, the flexibility of the process, examined the contrast generating potential of the nanodisco balls, evaluated whether the surface attachment of the IO-MHPC was robust to biological conditions *in vitro* and

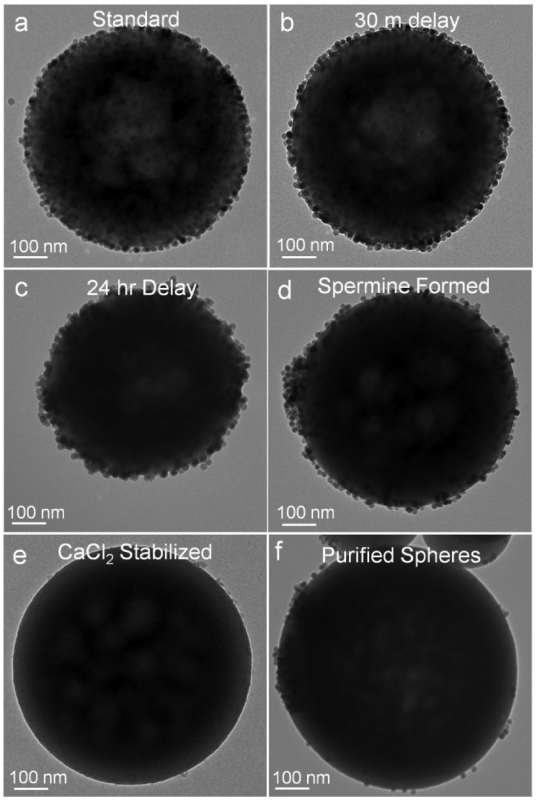

Figure 3. TEM images of synthesis variations: (a) standard synthesis, (b) 30 min and (c) 24 h preincubation of PCPP and IO-MHPC before spermine addition. TEM of (d) PCPP spheres formed with spermine and then incubated with IO-MHPC, (e) PCPP spheres formed with spermine, stabilized in $CaCl_2$ and then incubated with IO-MHPC, (f) purified nonloaded nanospheres subsequently loaded with IO-MHPC.

demonstrated the theranostic potential of the nanoparticles.

Surface Adhesion Occurs during Stabilization with $CaCl_2$. The surface loading of PCPP nanospheres occurs *via* self-assembly during synthesis. To investigate the crucial step in the formation of surface loaded nanospheres, we added IO-MHPC at different points in the process. Initially, we formed IO-NB by mixing IO-MHPC with a PCPP solution and then immediately adding spermine as schematically outlined in Figure 1b. The mixture was quickly transferred to a $CaCl_2$ solution and incubated at room temperature for 30 min. Afterward, the solution was washed through centrifugation and resuspended in water. To determine if longer incubations of IO-MHPC and PCPP solution together would result in internal loading of IO-MHPC, the reagents were incubated together at room temperature for 30 min and 24 h before the addition of spermine. Results in Figure 3a–c show no visible differences between our standard synthesis, 30 min preincubation, or 24 h preincubation, indicating that longer incubation times did not affect spatial distribution of IO-MHPC in PCPP nanospheres (Figure 3c).

Next, we examined the effect of mixing PCPP with spermine before the addition of IO-MHPC. As shown in Figure 3d, IO-MHPC surface adherence was unaffected when added after spermine addition, demonstrating that surface loading does not occur during the PCPP and spermine cross-linking process. To further explore the mechanism of surface loading, nonloaded spheres were completely formed before the addition of IO-MHPC. The PCPP solution and spermine were first mixed and then transferred to $CaCl_2$ for 30 min at room temperature. Afterward, IO-MHPC was added into the solution and stirred for an additional 30 min. The results seen in Figure 3e showed no surface loading of IO-MHPC in the sample. These data demonstrate that surface loading of MHPC lipid coated IONP (IO-MHPC) is achievable at any stage before $CaCl_2$ stabilization. We also found fully synthesized nonloaded nanospheres (nanospheres formed in the absence IO-MHPC) could be surface loaded by incubating the nonloaded spheres with IO-MHPC and then transferring to 0.88% $CaCl_2$ solution for 30 min Figure 3f). These data suggest a calcium-dependent mechanism for surface loading. Presumably, there is some form of calcium-mediated binding between the PCPP and phospholipid headgroup (Ca^{2+} binding to phospholipids is well-known).[36] Other divalent cations could likely produce similar phenomenon as Ca^{2+}.

With our standard synthesis method, we studied the IO-NB stability over time when stored in Milli-q water at room temperature. After 24 h, the IO-NB were found to loosely settle but could easily be redispersed with gently mixing. The surface loading and structure of these nanospheres was unaffected over the observed time frame of 7 months as determined by TEM (Figure S2, Supporting Information). These data indicate that the particles are robustly stable when stored at room temperature for extended periods of time.

Surface Loading Is Independent of Polymer Size, Lipid Length, Core Size, and Core Type. Exclusive surface loading was found with the use of MHPC lipids encapsulating 15.6 nm diameter iron nanoparticles. We examined the flexibility of the reaction by varying parameters such as PCPP molecular weight, phospholipid length, and nanocrystal core size and type. Surface loaded nanospheres were synthesized using our standard method with PCPP in a range of molecular weights (35.6 kDa, 1.0 MDa, 3.8 MDa MW). Surface loading of IO-MHPC was found with each PCPP MW, demonstrating that the process is independent of polymer size (Figure S3, Supporting Information). The effect of phospholipid tail length was studied by encapsulating 15.6 nm diameter IONP with 12 (LHPC), 14 (MHPC), 16 (PHPC), and 18 (SHPC) carbon tail chain length phospholipids. PCPP nanospheres were successfully synthesized and surface loaded with each micelle formation (Figure S4, Supporting Information, note that LHPC is a relatively poor amphiphile and therefore formed aggregates as opposed to individually dispersed nanocrystals). Additionally, oleate-coated IONP

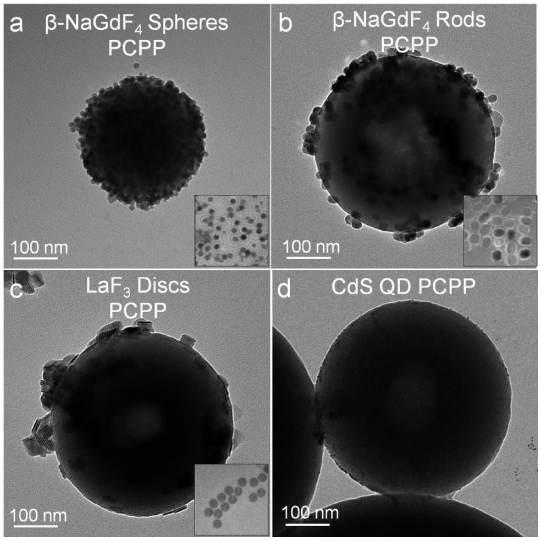

Figure 4. TEM images of PCPP nanosphere surface loaded with various nanocrystals: (a) β-$NaGdF_4$ spheres, (b) β-$NaGdF_4$ rods, (c) LaF_3 discs, and (d) CdS quantum dots surface loaded onto PCPP nanospheres (QD-NB).

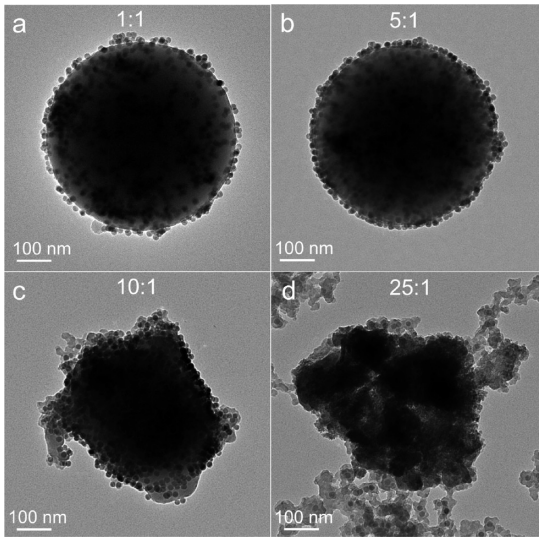

Figure 5. TEM images of PCPP nanosphere standard synthesis with increasing ratios of empty MHPC-micelles to IO-MHPC: (a) 1:1 (b) 5:1 (c) 10:1 (d) 25:1.

of increasing sizes (10, 15, 20, 25, 30 nm diameters) were encapsulated in micelles using MHPC/DMPC mixtures (IO-MHPC-DMPC). Micelles synthesized using only MHPC to encapsulate the larger 25 and 30 nm IONP were not stable; however, we found that they could be stably coated with a 1:1 mixture of MHPC/DMPC and that nanoparticles with such coatings adhered to PCPP nanospheres also. The PCPP nanospheres were synthesized using our standard method with the various IONP core sizes. TEM revealed surface loading occurred for each core size (Figure S5, Supporting Information).

To further explore the breadth of applicability of this surface loaded process, a variety of diagnostically active nanocrystals were investigated for adherence to PCPP nanospheres. Oleic acid coated quantum dots (CdS spheres) and nanophosphors (β-$NaGdF_4$ spheres, rods, LaF_3 discs) were all found to incorporate into MHPC micelles using the same procedure as for IONP. Surface loading of each core variant was achieved through our standard method of PCPP nanosphere synthesis. TEM verified surface adsorption to be present in each sample (Figure 4). From these data, it seems that nanocrystals encapsulated into phosphocholine headgroup lipid micelles can be successfully surface adsorbed onto PCPP nanospheres regardless of the core type, size, or shape.

Excess Empty Micelles Disrupt Nanosphere Formation but not Surface Adherence. We examined whether an excess of empty micelles would reduce surface adsorption of IO-MHPC on PCPP nanospheres. Empty MHPC micelles were mixed together with IO-MHPC at increasing ratios (1:1, 5:1, 10:1, 25:1, based on phospholipid content). PCPP nanosphere synthesis was performed using our standard method with these empty micelles:IO-MHPC ratios. From TEM, lower ratio mixtures did not appear to affect surface adsorption of IO-MHPC onto the PCPP nanospheres (Figure 5). However, at larger ratios of 10:1 and 25:1, disruption of nanosphere formation was observed. These particles appeared amorphous but the surface adsorption of the IO-MHPC was still present. The increased concentration of empty micelles appeared to interfere with the spermine-PCPP cross-linking. We hypothesized that performing the cross-linking before the addition of IO-MHPC and empty micelles would allow for the observation of competition without disrupting the PCPP nanosphere formation. We found that by adding the spermine before the IO-MHPC, we were able to surface load IO-MHPC in the presence of high concentrations of empty micelles. Ratios of 10:1, 15:1, 20:1, 25:1 were used in the synthesis, and surface loading of IO-MHPC appeared similar in all samples (Figure S6, Supporting Information). This phenomenon could be due to the larger area of interaction for the IO-MHPC with the PCPP nanospheres creating stronger attachments, therefore preferentially binding IO-MHPC as compared to empty MHPC micelles.

Particles Remain Diagnostically Active after Surface Loading. With the ability to load a variety of diagnostically active nanoparticles, we evaluated the contrast generating properties of nanocrystal loaded polymer particles. Magnetic moment curves measured for IO-MHPC and IO-NB did not indicate magnetic hysteresis (Figure 7, Supporting Information). IO-MHPC and IO-NB had almost identical magnetization saturation values of 67.81 and 65.01 emu/g, respectively. The longitudinal and transverse relaxivity (measures of MRI contrast) of surface loaded IO-NB were examined (Table 2) at 1.41 T and 37 °C. Surface loaded particles, IO-NB, were found to have a lower transverse (r_2) relaxivity than free

TABLE 2. Relaxation Measurements for Free IO-MHPC and IO-NB at 1.41 T

	r_1 (mM^{-1} s^{-1})	r_2 (mM^{-1} s^{-1})	r_2/r_1
IO-MHPC	3.95	107.66	27.3
IO-NB	1.81	68.22	37.6

IO-MHPC, although still at a substantial value of 68.2 mM^{-1} s^{-1}. The decreased relaxivity could be caused by some loss of interaction between the surrounding water due to the absorption of IO-MHPC to the PCPP nanospheres.[37] However, the ratio of transverse to longitudinal relaxivity (r_2/r_1) was higher for IO-NB indicating good properties for T_2-weighted imaging. Additionally, for further evaluation, contrast generation for IO-NB was evaluated with a MRI scan. Iron oxide increases the rate of transverse relaxation therefore leading to a decrease in signal intensity, or darkening in T_2/T_2*-weighted MR images. An MR image of a phantom containing IO-NB (0.05 and 0.16 mM Fe), DPBS, free IO-MHPC (0.16 mM Fe), and nonloaded PCPP spheres are displayed in Figure 6a. The DPBS and nonloaded PCPP nanospheres were of relatively similar signal intensity. As expected, the IO-NB were much darker, with a concentration-dependent intensity. Although the IO-NB and IO-MHPC samples were at the same concentration, the IO-NB produced less signal. This effect could be due to the increased relaxivity (r_2/r_1) ratio seen in the relaxation measurements or perhaps is due to the different field strengths used for imaging and to determine relaxivities. Overall, IO-NB retained relaxation properties that allow for contrast generation in MRI. Moreover, PCPP nanospheres loaded with quantum dots (QD-NB) exhibit similar fluorescent properties as free quantum dots (QD-MHPC). The fluorescence of the quantum dots persisted after encapsulation in micelles and PCPP surface loading (Figure 6b). The phantom image in Figure 6c indicates the strong CT contrast produced by gold loaded PCPP particles.

***In Vitro* Evaluation of Surface Loaded Nanospheres.** The robustness of surface attachment of IO-MHPC to PCPP nanospheres was briefly evaluated for potential biological applications. We incubated nanodisco balls for 1, 4, and 24 h in cell culture media at 37 °C. IO-NB were then collected through centrifugation, and iron oxide content was measured through ICP-OES (Figure 7a). The loss of iron content in the samples appeared similar at each time point, suggesting that after some initial IO-MHPC release the remainder was retained over the time frame tested. TEM performed on these nanoparticles revealed that many IO-MHPC were still attached to the surface of PCPP nanospheres after 4 h incubation (Figure 7b). Next, we incubated IO-NB with RAW 264.7 monocytes for 4 h. Remarkably, TEM performed on these cells revealed IO-MHPC organized

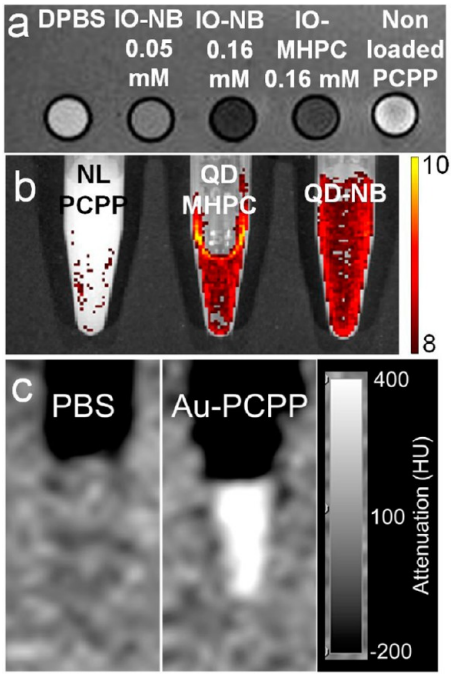

Figure 6. Applications of surface loaded PCPP nanospheres: (a) MRI phantom image, (b) fluorescence image of nonloaded PCPP particles, QD-MHPC micelles, and QD-NB. Scale bar in units of radiant efficiency ($\times 10^7$ (p/s/cm^2/sr)/μW/cm^2). (c) CT phantom image of gold loaded PCPP particles (17 mg/mL).

in ring shapes located within endosomes (Figure 7c). We believe this demonstrates that the IO-MHPC still remain surface bound to PCPP nanospheres after undergoing cellular uptake.

Delivery of Protein Loaded IO-NB. With exclusive surface loading of polymer nanospheres, the internal core of the nanospheres can be used for drug loading. We used bovine serum albumin conjugated with fluorescein isothiocyanate (FITC-BSA, 0.25 mg) as a model drug. This was loaded into PCPP nanospheres (FITC-PCPP). Additionally, FITC-BSA was loaded into the core of nanospheres with simultaneous surface loading of IO-MHPC (FITC-NB, 0.1, 0.25 mg). TEM and fluorescence imaging were used to characterize FITC-PCPP and FITC-NB. Both particles demonstrated successful loading of FITC-BSA into the PCPP nanosphere as evident from the fluorescence of the purified material. TEM of FITC-NB revealed that IO-MHPC were surface loaded in the presence of the additional FITC-BSA payload, without alteration of the NB structure (Figure S8, Supporting Information).

To evaluate the ability of these particles to deliver FITC-BSA to cells, they were incubated with monocytes for 4 h. Afterward the cells were stained with DAPI and imaged with fluorescence microscopy. Phase images of treated cells reveal areas of particle uptake within the cells (Figure 8). Additionally, FITC can be seen within the cells as defined by DAPI (nuclei stain). The added surface loaded IO-MHPC did not prevent the

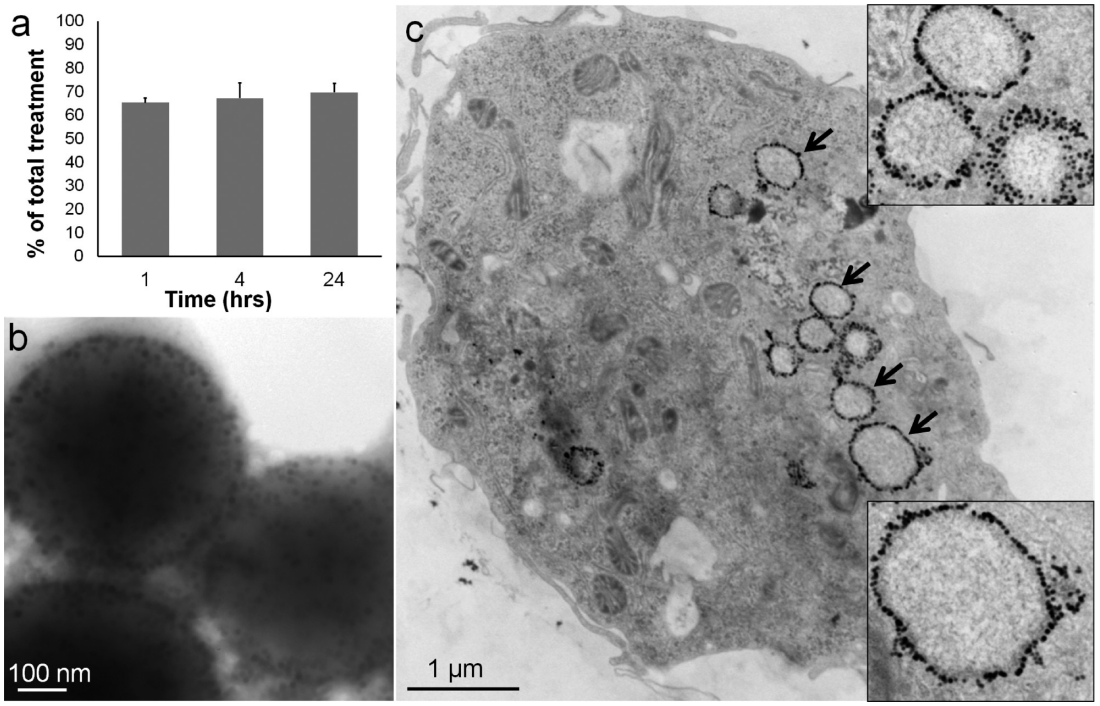

Figure 7. IO-NB stability and uptake for cell studies. (a) Remaining iron oxide concentration after incubation in serum for 1, 4, and 24 h. (b) TEM image of IO-NB incubated for 4 h in cell culture media. (c) TEM images of macrophages that have been incubated with IO-NB. Arrows indicate areas of IO-NB uptake.

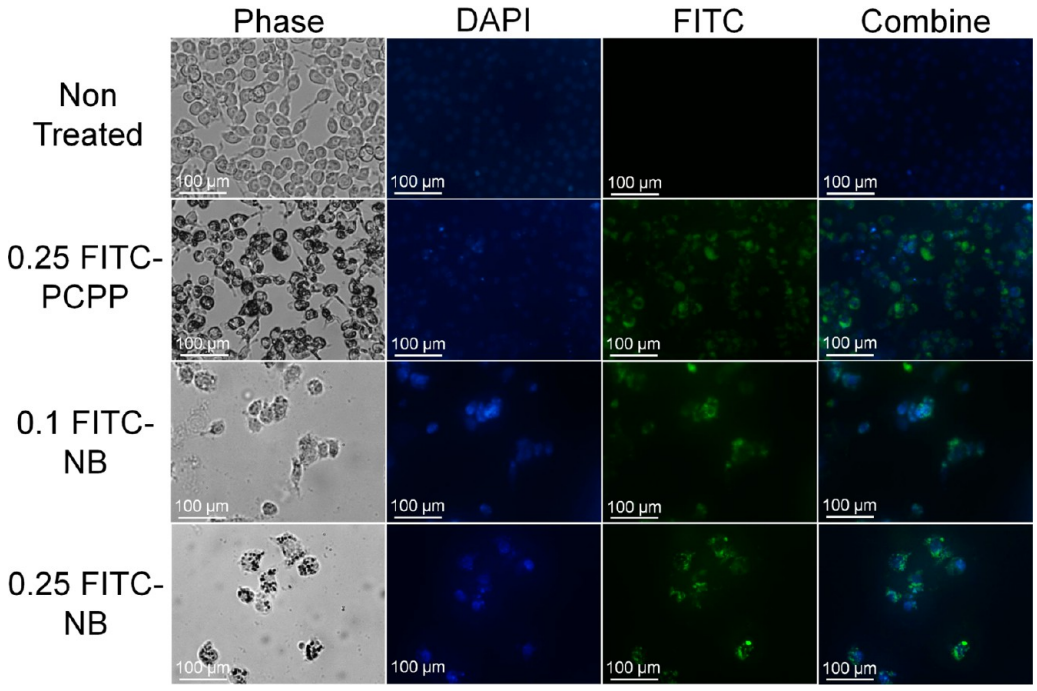

Figure 8. Fluorescence of monocytes treated with FITC-BSA encapsulated PCPP nanospheres. Images of phase, DAPI (blue), FITC (green), and the combination of DAPI and FITC for the conditions indicated after 4 h.

delivery of FITC-BSA to the cells. These data demonstrate that "drug" (FITC-BSA) loading can be achieved with additional exclusive surface loading. Furthermore, the loaded nanospheres remained stable for *in vitro* tracking of delivery into cells.

CONCLUSIONS

As we have described above, PCPP nanospheres can be loaded with nanocrystals in a controlled fashion to result in exclusive localization of the nanocrystals to the surface of the sphere rather than the typically

observed core loading of polymer nanoparticles. We found that simultaneous surface and core loading is possible. A range of diagnostically active nanocrystals could be surface loaded onto the PCPP nanospheres regardless of their individual core size, shape, or chemical composition. The nanocrystals loaded on the spheres retained their contrast generating properties, *i.e.*, MR contrast for iron oxide particles and fluorescence for quantum dots. The point of nanocrystal attachment was also probed through the investigation of each synthesis step. We observed that surface loading was successful prior to $CaCl_2$ addition. In addition, we found that surface loading was achievable using a variation of polymer sizes and phospholipid tail lengths, demonstrating multiple feasible approaches to surface loading. We showed the stability of the nanodisco balls in cell culture media and the potential for drug delivery applications. In summary, we have presented a robust and unique platform for surface localization of nanoparticles onto a polymeric sphere to form "nanodisco balls". Selective loading into the core and surface presents new opportunities in the areas of drug delivery and theranostics.

MATERIALS AND METHODS

Materials. Poly(bis(4-carboxyphenoxy)phosphazene) disodium salt (PCPP, 1 MDa) was purchased from Sigma-Aldrich (St. Louis, MO). PCPP polymers of 3.8 MDa and 36.4 kDa molecular weight were synthesized at the Pennsylvania State University. All phospholipids including 1-myristoyl-2-hydroxy-*sn*-glycero-3-phosphocholine (MHPC) and chain length variants were purchased from Avanti Polar Lipids (Alabaster, AL). Oleic acid capped cadmium sulfide quantum dots were purchased from NN-Laboratories, LLC (Fayettville, AR). Oleic acid capped iron oxide nanoparticles (IONP) of various sizes (10, 15, 20, 25, 30 nm) were purchased from Ocean NanoTech (Springdale, AR), and some IONP were synthesized at the University of Pennsylvania (*vide infra*). All other chemicals of analytical grade were purchased through Sigma-Aldrich (St. Louis, MO) with the exceptions of sodium fluoride (Acros Organics, NJ), trifluoroacetic acid (Alfa Aesar, MA), Tetrahydrofuran (EMD, PA), dichloromethane (EMD, PA), and ethyl ether (EMD, PA). Gadolinium or lanthanum trifluoroacetate precursors were prepared using a literature method by refluxing gadolinium or lanthanum oxide in trifluoroacetic acid/water mixture (50 vol %).[38] A monocyte cell line, RAW 264.7, was purchased from ATCC. Cells were cultured in Dubecco's Modified Eagle Medium supplemented with 10% fetal bovine serum and 1% penicillin/streptomycin (10000 units/mL, 10000 μg/mL) from Life Technologies Invitrogen (Grand Island, NY).

Polyphosphazene Synthesis. For 35.6 kDa PCPP preparation, PCl_5 (0.11 g) was dissolved in 50 mL of anhydrous dichloromethane (DCM) for 10 min. Chlorophosphoranimine (6.00 g), prepared as previously reported,[38] was added to the solution rapidly, and the mixture was stirred at room temperature for 4 h. DCM was then removed under reduced pressure to give colorless viscous living oligo(dichlorophosphazene). The polymer was redissolved in anhydrous tetrahydrofuran (THF), and propyl 4-hydroxybenzoate (14.43 g) and $CsCO_3$ (26.00 g) were added to the solution. The mixture was stirred at room temperature for 2 days. Afterward, the reaction medium was concentrated and precipitated into water (300 mL $\times$ 3). The precipitate was isolated by centrifugation. Then, the crude product was redissolved in DCM and dialyzed *versus* methanol/DCM (1:4) for 3 days (Spectra/Por dialysis membrane, MWCO: 1000). The solvent was removed under vacuum to give a white adhesive polymer. (Molecular weight: 35.6 g/mol; PDI: 1.07; repeat units: 82) For the deprotection reaction, the above 1.00 g of polymer was dissolved in 100 mL of anhydrous THF. Potassium *tert*-butoxide (2.50 g) and water (0.45 g) were added to the polymer solution. The mixture was stirred at room temperature for 3 days. Then, the reaction medium was dialyzed *versus* water for 1 day, water/methanol (1:1) for 2 days, and then methanol for 2 days (Spectra/Por dialysis membrane, MWCO: 1000). Poly(bis(4-carboxylatophenoxy)phosphazene) dipotassium was obtained by the removal of all solvent under vacuum at 35 °C (overall yield: 46%). ^{31}P NMR (D_2O): δ −18.75 (s). ^{1}H NMR (D_2O): δ 7.31 (d, 2H), 6.50 (d, 2H).

A high molecular weight (MW) PCPP (3.8 MDa) was synthesized by first dissolving poly(dichlorophophazene) (2.00 g) in 200 mL of THF. Poly(dichlorophosphazene) was prepared by the thermal ring-opening polymerization of recrystallized and sublimed hexachlorocyclotriphosphazene (Fushimi Chemical Co., Japan) in evacuated Pyrex tubes at 250 °C. Propyl-4-hydroxybenzoate (9.33 g) was dissolved in THF (100 mL) and then added to the polymer solution. Solid cesium carbonate (16.9 g) was then immediately added to the reaction mixture. The reaction proceeded at room temperature for 3 days. Afterward, the solution was concentrated and precipitated into water 3 times and hexane once. The solvent was removed under reduced pressure to yield a white solid that was obtained in an 80% yield (molecular weight: 3882000 g/mol; PDI: 1.62; repeat units: 9600). For the deprotection reaction, the polymer (3.00 g) was redissolved in anhydrous THF (300 mL). Potassium *tert*-butoxide (7.51 g) and water (1.34 g) were added to the polymer solution. The reaction was stirred at room temperature for 3 days and was then concentrated. This was dialyzed versus water for 2 days, (1:1) methanol/water for 2 days, and then (4:1) methanol/water for 1 day. The solvent was then removed under reduced pressure to yield the product with an 81% yield. ^{31}P NMR (D2O): δ −18.53 (s). ^{1}H NMR (D2O): 7.16 (s, 2H), 6.36 (s, 2H).

Iron Oxide Synthesis. Iron oxide nanoparticles (IONP) were synthesized using oleic acid as the capping ligand following a modified literature method.[39] Typically, 1.5 g of iron chloride and 5.2 g of sodium oleate were first added in a 100 mL flask. Subsequently, 20 mL of hexane, 11.5 mL of ethanol, and 8.8 mL of distilled water were added to the flask, and the mixture was sonicated. The two-phase mixture was heated to reflux (~70 °C) for 4 h, which produced iron oleate in the organic layer. The upper organic layer was washed three times with 30 mL of water and separated by centrifugation (5000 rpm, 10 min). After washing, the hexane was evaporated from the dark brown organic layer and stored under vacuum. The synthesis of 15.6 nm iron oxide nanoparticles was carried out by reacting 5.5 g of iron oleate and 1.5 g of oleic acid in 31 g of 1-octadecene in a 250 mL round-bottom flask. The reaction mixture was heated to 320 °C at a rate of 200 °C/h and kept at that temperature for 30 min. The color of the solution turned from dark brown to black upon the formation of nanoparticles. The resulting solution was cooled to room temperature, and nanoparticles were precipitated by adding ethanol (35 mL). The precipitated nanoparticles were collected by centrifugation (5000 rpm, 10 min) and then redispersed in hexane (10 mL). The nanoparticles were further purified by precipitation with acetone (35 mL), centrifuging at 5000 rpm for 10 min, and redispersing the collected nanoparticles in hexane (10 mL). This washing step was repeated two more times. After the final washing step, the IONP were redissolved in chloroform (10 mL) and centrifuged at low speed (3000 rpm, 5 min) to remove aggregates. A sample of these IONP was rendered water-soluble through encapsulation with dimercaptosuccinic acid (Figure S9a, Supporting Information) following previous literature methods (IODMSA).[40]

Gold Nanoparticle Synthesis. Carboxylic-acid coated gold nanoparticles (AuNP) were synthesized using the Turkevich method with slight modifications.[41] Briefly, 85 mg of chloroauric acid ($HAuCl_3$) was dissolved in 250 mL of Milli-Q water for a final concentration of 1 mM. After heating to a boil, a 38.8 mM solution of sodium citrate (285 mg in 25 mL Milli-Q water) was added, causing the color of the solution to become dark red. The solution was heated for another 15 min and then allowed to cool to room temperature. For carboxylic acid ligand exchange, an 11.9 mM solution of 11-mercaptoundecanoic acid (11-MUA, 2.6 mg in 1 mL of EtOH) was added to the citrate AuNP as prepared above. The solution was stirred for 24 h. Afterward, the AuNP were purified and collected by centrifuging at 12.5 krcf for 45 min. The pellet was resuspended with Milli-Q water and repeated two times. The AuNP solution was finally resuspended in 1 mL of Milli-Q water and filtered through a 0.45 μm syringe filter.

Nanophosphor Synthesis. Hexagonal phase sodium gadolinium tetrafluoride nanospheres (β-$NaGdF_4$) were synthesized according to a previously reported procedure with slight modification.[42] Briefly, gadolinium trifluoroacetate (2 mmol) and sodium fluoride (5 mmol) were added into a 125 mL three-neck flask containing 60 mL of 1-octadecene/oleic acid solvent mixture (50% by volume). The solution was then degassed under vacuum at 125 °C for 1 h to remove water. For nanocrystal growth, the solution was heated to 290 °C under N_2 environment at a rate of 10 °C/min and maintained at this temperature for 5 h. Purification was performed twice by washing with ethanol and then centrifuging at 6000 rpm for 2 min. The nanocrystals were redissolved in hexane (10 mL), and residual sodium fluoride was removed by centrifugation at 3000 rpm for 2 min. β-$NaGdF_4$ nanorods were synthesized by using 2.5 mmol of sodium fluoride *via* the same method to synthesize nanospheres. Lanthanum trifluoride (LaF_3) discs were synthesized using similar methods as β-$NaGdF_4$ nanospheres while substituting lanthanum trifluoroacetate for gadolinium trifluoroacetate. The reactions were conducted at 290 °C for 5 h under a N_2 environment. LaF_3 nanoplates were redissolved in hexane and centrifuged at 3000 rpm for 2 min to remove lithium fluoride salts.

Nanocrystal Micelle Synthesis. IONP, quantum dots, and nanophosphors were rendered water-soluble through encapsulation in phospholipid micelles. In a typical preparation, 50 mg of MHPC (Figure S9b, Supporting Information) was dissolved in a 1 mL chloroform/methanol mixture (4:1). Oleic acid coated IONP (5.00 mg in 0.5 mL of chloroform) were added to the MHPC solution. This mixture was then added to heated Milli-Q water (10 mL) in a slow, dropwise fashion. The resulting solution was heated for an additional 10 min to ensure organic solvent evaporation and then cooled to room temperature. Afterward, the aqueous solution was centrifuged at 800*g* for 10 min to remove precipitates and multicored micelles. The supernatant was collected and centrifuged at 20000*g* for 90 min. The pellet was redispersed in Milli-Q water (~15 mL). These washes were performed three times to ensure purification. Finally, the sample was resuspended in approximately 1 mL of Mill-Q water yielding IONP encapsulated in MHPC micelles (IO-MHPC). Quantum dots and nanophosphors were encapsulated using similar methods as the IONP. Iron oxide encapsulation was also performed using the following additional lipids: 1-lauroyl-2-hydroxy-*sn*-glycero-3-phosphocholine (IO-LHPC), 1-palmitoyl-2-hydroxy-*sn*-glycero-3-phosphocholine (IO-PHPC), and 1-stearoyl-2-hydroxy-*sn*-glycero-3-phosphocholine (IO-SHPC). Additionally, MHPC micelles were formed in the absence of any nanocrystals to obtain samples of empty MHPC micelles. Mixed phospholipid micelles encapsulating IONP (10, 15, 20, 25, and 30 nm diameter) were formed with a 1:1 mixture of MHPC and dimyristoyl-2-hydroxy-*sn*-glycero-3-phosphocholine (DMPC, Figure S9c, Supporting Information).

PCPP Sphere Synthesis. Formation of polyphosphazene polymer nanospheres was performed using modified literature methods.[28,30] A typical synthesis was performed as follows, 40.0 mg of PCPP (1.0 MDa MW) was dissolved in 20 mL of Dulbecco's phosphate buffered saline (DPBS, pH 7.4). IO-MHPC (0.15 mg, 200 μL) were added into 1 mL of this PCPP solution. Then 16.8 μL of a 70.0 mg/mL spermine solution (DPBS, pH 7.4) was added to the PCPP/IO-MHPC solution (0.98% spermine). The mixture was immediately added into a beaker of 88.0 mg/mL $CaCl_2$ buffer (~100 mL) and incubated at room temperature for 30 min while stirring. This suspension was purified through centrifugation (800*g*, 10 min) and washed three times with Milli-Q water. The resulting IO-MHPC surface loaded nanospheres (IO-NB) were resuspended in 1 mL of Milli-Q water. This process is depicted schematically in Figure 1b. Syntheses of nonloaded PCPP nanospheres were formed similarly, except without the addition of IO-MHPC. PCPP nanospheres (AuIO-NB) were formed, for example, by mixing IO-MHPC (0.15 mg, 42 μL) and AuNP (1 mg, 32 μL) together. Afterward, this solution was added to 1 mL of previously described PCPP solution. The synthesis followed as described above. Nanocrystal variants such as CdS quantum dots, nanophosphors (β-$NaGdF_4$ spheres, rods, LaF_3 discs), or iron oxides of varying cores sizes and coatings were substituted for IO-MHPC for inclusion in the PCPP nanosphere synthesis. PCPP of additional molecular weights (35.6 kDa and 3.88 MDa) were also used to form surface loaded nanospheres. Additionally, FITC-BSA (0.1, 0.25 mg) was core loaded into PCPP nanospheres using the standard synthesis method with and without the simultaneous surface loading of IO-MHPC (0.15 mg) to form FITC-PCPP and FITC-NB, respectively.

Polymer and Particle Characterization. ^1H and ^{31}P NMR spectra were recorded on a Bruker WM-360 NMR spectrometer operated at 360 and 145 MHz, respectively. ^1H NMR spectra were referenced to solvent signals, while ^{31}P NMR chemical shifts were relative to 85% phosphoric acid as an external reference, with positive shift values downfield from the reference. Molecular weights were estimated using a Hewlett-Packard HP 1090 gel permeation chromatograph (GPC) equipped with an HP-1047A refractive index detector, American Polymer Standards AM gel 10 mm and AM gel 10 mm 104 Å columns, and calibrated versus polystyrene standards.

Transmission electron microscopy images were acquired on a FEI Tecnai T12 microscope at 120 kV. Scanning electron microscopy was performed with a Philips XL20 at 10 kV. Fluorescent imaging for both the quantum dots and the FITC-BSA was performed with an IVIS Spectrum system using 465 nm excitation and 520 nm emission filters. Relaxivities were measured using a Bruker Minispec mq relaxometer at 1.41 T (60 MHz) and 40 °C. Freely suspended IO-MHPC were prepared in DPBS for measurements. PCPP samples were prepared in a 1% agar gel in DPBS to prevent sedimentation of nanospheres. Iron oxide concentrations were determined through inductively coupled plasma-optical emission spectroscopy (ICP-OES) on a Spectro Genesis system.

Magnetic hysteresis measurements were performed on a MicroMag Magnetometer (Westerville, OH) at a field range of 10 kOe. Samples (5 μL) were prepared on a coverglass for measurements. Magnetic resonance imaging (MRI) was used to evaluate IO-NB contrast generating properties. IO-NB were prepared in a 1% agar gel at concentrations of 0.05 mM and 0.16 mM of Fe. Additionally, control samples of DPBS, nonloaded PCPP, and 0.16 mM of Fe IO-MHPC in 1% agar gel were scanned. For MRI phantom preparation, samples were placed in a 2% agar gel doped with 0.35 mM manganese chloride. The samples were scanned using a head coil on a Siemens Magnetom Trio with a 3 T magnet. A 2D spin echo sequence was used. Relevant imaging parameters were as follows: echo time (TE), 15 ms; repetition time (TR), 10 s; 1 slice with thickness 3 mm, 1 average, flip angle (FA), 90 deg; acquisition matrix, 184 × 256; in-plane spatial resolution 0.546 mm^2, field of view (FOV) 140 mm^2. The resulting images were processed using Osirix v.3.0.1 32-bit (Geneva, Switzerland; www.osirix-viewer.com). CT images were acquired with a Siemens Definition DS 64-slice clinical CT scanner at 140 kV (245 mA) with a matrix size of 512 × 512, field of view 37 × 37 cm, reconstruction kernel B30f, and slice thickness of 0.6 cm. Images were analyzed using Osirix 64 bit (v3.7.1).

***In Vitro* Incubations.** RAW 264.7 cells were cultured on 6-well plates at a concentration of 2 million cells/mL at 37 °C. After 24 h, the cells were treated with IO-NB at a concentration of 50 μg of Fe/mL (0.89 mM) for 4 h. The cells were washed 3 times with DPBS and then collected by gentle scraping. The cells were

fixed in a solution of 2% glutaraldehyde and 5% paraformaldehyde in DPBS. Fixed cells were embedded in resin and prepared for TEM using standard methods.[43] Cell sections were imaged using a FEI Tecnai T12 electron microscope.

For fluorescent microscopy, RAW 264.7 cells were cultured on glass-bottomed well dishes (20 mm diameter) at a concentration of 800*K* cells per well. After 24 h, the cells were treated with 50 μg Fe/ml (0.89 mM) of FITC-NB or FITC-PCPP for 4 h. The cells were then washed with DPBS 3 times and stained with DAPI. Imaging was performed on a Nikon Eclipse fluorescence microscope (Nikon Eclipse Ti-U, Melville, NY). The DAPI stain was imaged using a 358 nm excitation filter and a 461 nm emission filter. FITC was imaged using a 494 nm excitation filter and a 516 nm emission filter.

Conflict of Interest: The authors declare no competing financial interest.

Acknowledgment. This work was supported by R00 EB012165 (D.P.C.) and T32 HL007954 (P.C). We also thank the University of Pennsylvania for startup funding. The project described was supported in part by Grant No. UL1RR024134 from the National Center for Research Resources. The content is solely the responsibility of the authors and does not necessarily represent the official views of the National Center for Research Resources or the National Institutes of Health. Supported in part by the Institute for Translational Medicine and Therapeutics' (ITMAT) Transdisciplinary Program in Translational Medicine and Therapeutics. We thank A. Andrianov for helpful suggestions with regard to PCPP sphere synthesis and M. Chorny for his help with magnetic moment measurements.

Supporting Information Available: TEM of gold nanocrystal loaded particles, the TEM results of IO-NB stability over time, synthesis for varied polymer molecular weight, phospholipid coatings, iron oxide core sizes, and excess phospholipids incubation. Magnetic hysteresis curves and characterization of FITC-BSA containing particles. Chemical structures of the capping ligands and phospholipids used for micelle formation. Videos of TEM tilt series with disco ball. This material is available free of charge *via* the Internet at http://pubs.acs.org.

REFERENCES AND NOTES

1. Li, N.; Zhao, P.; Astruc, D. Anisotropic Gold Nanoparticles: Synthesis, Properties, Applications, and Toxicity. *Angew. Chem.* **2014**, *53*, 1756–1789.
2. Nehl, C. L.; Liao, H.; Hafner, J. H. Optical Properties of Star-Shaped Gold Nanoparticles. *Nano Lett.* **2006**, *6*, 683–688.
3. Kim, J.; Park, S.; Lee, J. E.; Jin, S. M.; Lee, J. H.; Lee, I. S.; Yang, I.; Kim, J.-S.; Kim, S. K.; Cho, M.-H.; *et al.* Designed Fabrication of Multifunctional Magnetic Gold Nanoshells and Their Application to Magnetic Resonance Imaging and Photothermal Therapy. *Angew. Chem., Int. Ed.* **2006**, *45*, 7754–7758.
4. Skrabalak, S. E.; Chen, J.; Sun, Y.; Lu, X.; Au, L.; Cobley, C. M.; Xia, Y. Gold Nanocages: Synthesis, Properties, and Applications. *Acc. Chem. Res.* **2008**, *41*, 1587–1595.
5. Liu, P.; Hensen, E. J. Highly Efficient and Robust Au/$MgCuCr_2O_4$ Catalyst for Gas-Phase Oxidation of Ethanol to Acetaldehyde. *J. Am. Chem. Soc.* **2013**, *135*, 14032–14035.
6. Wu, Z.; Song, T.; Xia, Z.; Wei, H.; Sun, B. Enhanced Performance of Polymer Solar Cell with Zno Nanoparticle Electron Transporting Layer Passivated by *in Situ* Cross-Linked Three-Dimensional Polymer Network. *Nanotechnology* **2013**, *24*, 484012.
7. Zhou, W.; Gao, P.; Shao, L.; Caruntu, D.; Yu, M.; Chen, J.; O'Connor, C. J. Drug-Loaded, Magnetic, Hollow Silica Nanocomposites for Nanomedicine. *Nanomedicine* **2005**, *1*, 233–237.
8. Mieszawska, A. J.; Kim, Y.; Gianella, A.; van Rooy, I.; Priem, B.; Labarre, M. P.; Ozcan, C.; Cormode, D. P.; Petrov, A.; Langer, R.; *et al.* Synthesis of Polymer−Lipid Nanoparticles for Image-Guided Delivery of Dual Modality Therapy. *Bioconjugate Chem.* **2013**, *24*, 1429–1434.
9. Mieszawska, A. J.; Gianella, A.; Cormode, D. P.; Zhao, Y. M.; Meijerink, A.; Langer, R.; Farokhzad, O. C.; Fayad, Z. A.; Mulder, W. J. M. Engineering of Lipid-Coated PLGA Nanoparticles with a Tunable Payload of Diagnostically Active Nanocrystals for Medical Imaging. *Chem. Commun.* **2012**, *48*, 5835–5837.
10. Jennings, T. L.; Singh, M. P.; Strouse, G. F. Fluorescent Lifetime Quenching near D = 1.5 nm Gold Nanoparticles: Probing Nset Validity. *J. Am. Chem. Soc.* **2006**, *128*, 5462–5467.
11. Binder, W. H.; Sachsenhofer, R.; Farnik, D.; Blaas, D. Guiding the Location of Nanoparticles into Vesicular Structures: A Morphological Study. *Phys. Chem. Chem. Phys.* **2007**, *9*, 6435–6441.
12. Kalra, V.; Lee, J.; Lee, J. H.; Lee, S. G.; Marquez, M.; Wiesner, U.; Joo, Y. L. Controlling Nanoparticle Location Via Confined Assembly in Electrospun Block Copolymer Nanofibers. *Small* **2008**, *4*, 2067–2073.
13. Mai, Y.; Eisenberg, A. Controlled Incorporation of Particles into the Central Portion of Vesicle Walls. *J. Am. Chem. Soc.* **2010**, *132*, 10078–10084.
14. Krack, M.; Hohenberg, H.; Kornowski, A.; Lindner, P.; Weller, H.; Forster, S. Nanoparticle-Loaded Magnetophoretic Vesicles. *J. Am. Chem. Soc.* **2008**, *130*, 7315–7320.
15. Pinho, S. L. C.; Laurent, S.; Rocha, J.; Roch, A.; Delville, M. H.; Mornet, S.; Carlos, L. D.; Vander Elst, L.; Muller, R. N.; Geraldes, C. F. G. C. Relaxometric Studies of Gamma-Fe_2O_3@SiO_2 Core Shell Nanoparticles: When the Coating Matters. *J. Phys. Chem. C* **2012**, *116*, 2285–2291.
16. van Schooneveld, M. M.; Gloter, A.; Stephan, O.; Zagonel, L. F.; Koole, R.; Meijerink, A.; Mulder, W. J.; de Groot, F. M. Imaging and Quantifying the Morphology of an Organic-Inorganic Nanoparticle at the Sub-Nanometre Level. *Nat. Nanotechnol.* **2010**, *5*, 538–544.
17. Wijaya, A.; Hamad-Schifferli, K. High-Density Encapsulation of Fe_3O_4 Nanoparticles in Lipid Vesicles. *Langmuir* **2007**, *23*, 9546–9550.
18. Luo, Q. J.; Hickey, R. J.; Park, S. J. Controlling the Location of Nanoparticles in Colloidal Assemblies of Amphiphilic Polymers by Tuning Nanoparticle Surface Chemistry. *ACS Macro Lett.* **2013**, *2*, 107–111.
19. Allcock, H. R. *Chemistry and Applications of Polyphosphazenes*; Wiley-Interscience: Hoboken, NJ, 2003; p xi, 725 p.
20. Kumbar, S. G.; Bhattacharyya, S.; Nukavarapu, S. P.; Khan, Y. M.; Nair, L. S.; Laurencin, C. T. *In Vitro* and *in Vivo* Characterization of Biodegradable Poly(Organophosphazenes) for Biomedical Applications. *J. Inorg. Organomet. Polym.* **2006**, *16*, 365–385.
21. Allcock, H. R.; Morozowich, N. L. Bioerodible Polyphosphazenes and Their Medical Potential. *Polym. Chem.* **2012**, *3*, 578–590.
22. Lakshmi, S.; Katti, D. S.; Laurencin, C. T. Biodegradable Polyphosphazenes for Drug Delivery Applications. *Adv. Drug. Delivery Rev.* **2003**, *55*, 467–482.
23. Andrianov, A. K.; Payne, L. G.; Visscher, K. B.; Allcock, H. R.; Langer, R. Hydrolytic Degradation of Ionically Cross-Linked Polyphosphazene Microspheres. *J. Appl. Polym. Sci.* **1994**, *53*, 1573–1578.
24. Singh, A.; Krogman, N. R.; Sethuraman, S.; Nair, L. S.; Sturgeon, J. L.; Brown, P. W.; Laurencin, C. T.; Allcock, H. R. Effect of Side Group Chemistry on the Properties of Biodegradable L-Alanine Cosubstituted Polyphosphazenes. *Biomacromolecules* **2006**, *7*, 914–918.
25. Allcock, H. R.; Kwon, S. An Ionically Cross-Linkable Polyphosphazene - Poly[Bis(Carboxylatophenoxy)Phosphazene] and Its Hydrogels and Membranes. *Macromolecules* **1989**, *22*, 75–79.
26. Allcock, H. R.; Kwon, S.; Riding, G. H.; Fitzpatrick, R. J.; Bennett, J. L. Hydrophilic Polyphosphazenes as Hydrogels: Radiation Cross-Linking and Hydrogel Characteristics of Poly[Bis(Methoxyethoxyethoxy)Phosphazene]. *Biomaterials* **1988**, *9*, 509–513.
27. Andrianov, A. K.; DeCollibus, D. P.; Gillis, H. A.; Kha, H. H.; Marin, A.; Prausnitz, M. R.; Babiuk, L. A.; Townsend, H.; Mutwiri, G. Poly[Di(Carboxylatophenoxy)Phosphazene]

Is a Potent Adjuvant for Intradermal Immunization. *Proc. Natl. Acad. Sci. U.S.A.* **2009**, *106*, 18936–18941.
28. Andrianov, A. K.; Chen, J. P. Polyphosphazene Microspheres: Preparation by Ionic Complexation of Phosphazene Polyacids with Spermine. *J. Appl. Polym. Sci.* **2006**, *101*, 414–419.
29. Garlapati, S.; Eng, N. F.; Wilson, H. L.; Buchanan, R.; Mutwiri, G. K.; Babiuk, L. A.; Gerdts, V. Pcpp (Poly[Di-(Carboxylatophenoxy)-Phosphazene]) Microparticles Co-Encapsulating Ovalbumin and CpG Oligo-Deoxynucleotides Are Potent Enhancers of Antigen Specific Th1 Immune Responses in Mice. *Vaccine* **2010**, *28*, 8306–8314.
30. Andrianov, A. K.; Chen, J.; Payne, L. G. Preparation of Hydrogel Microspheres by Coacervation of Aqueous Polyphosphazene Solutions. *Biomaterials* **1998**, *19*, 109–115.
31. Cormode, D. P.; Sanchez-Gaytan, B. L.; Mieszawska, A. J.; Fayad, Z. A.; Mulder, W. J. M. Inorganic Nanocrystals as Contrast Agents in MRI: Synthesis, Coating and Introduction of Multifunctionality. *NMR Biomed.* **2013**, *26*, 766–780.
32. Skajaa, T.; Cormode, D. P.; Jarzyna, P. A.; Delshad, A.; Blachford, C.; Barazza, A.; Fisher, E. A.; Gordon, R. E.; Fayad, Z. A.; Mulder, W. J. The Biological Properties of Iron Oxide Core High-Density Lipoprotein in Experimental Atherosclerosis. *Biomaterials* **2011**, *32*, 206–213.
33. van Schooneveld, M. M.; Vucic, E.; Koole, R.; Zhou, Y.; Stocks, J.; Cormode, D. P.; Tang, C. Y.; Gordon, R. E.; Nicolay, K.; Meijerink, A.; *et al.* Improved Biocompatibility and Pharmacokinetics of Silica Nanoparticles by Means of a Lipid Coating: A Multimodality Investigation. *Nano Lett.* **2008**, *8*, 2517–2525.
34. Cormode, D. P.; Naha, P. C.; Fayad, Z. A. Nanoparticle Contrast Agents for Computed Tomography: A Focus on Micelles. *Contrast Media Mol. Imaging* **2014**, *9*, 37–52.
35. Galper, M. W.; Saung, M. T.; Fuster, V.; Roessl, E.; Thran, A.; Proksa, R.; Fayad, Z. A.; Cormode, D. P. Effect of Computed Tomography Scanning Parameters on Gold Nanoparticle and Iodine Contrast. *Invest. Radiol.* **2012**, *47*, 475–481.
36. Macdonald, P. M.; Seelig, J. Calcium-Binding to Mixed Phosphatidylglycerol-Phosphatidylcholine Bilayers as Studied by Deuterium Nuclear-Magnetic-Resonance. *Biochemistry* **1987**, *26*, 1231–1240.
37. Bjornerud, A.; Johansson, L. The Utility of Superparamagnetic Contrast Agents in MRI: Theoretical Consideration and Applications in the Cardiovascular System. *NMR Biomed.* **2004**, *17*, 465–477.
38. Wang, B.; Rivard, E.; Manners, I. A New High-Yield Synthesis of Cl(3)P=NSiMe(3), a Monomeric Precursor for the Controlled Preparation of High Molecular Weight Polyphosphazenes. *Inorg. Chem.* **2002**, *41*, 1690–1691.
39. Park, J.; An, K.; Hwang, Y.; Park, J. G.; Noh, H. J.; Kim, J. Y.; Park, J. H.; Hwang, N. M.; Hyeon, T. Ultra-Large-Scale Syntheses of Monodisperse Nanocrystals. *Nat. Mater.* **2004**, *3*, 891–895.
40. Jun, Y. W.; Huh, Y. M.; Choi, J. S.; Lee, J. H.; Song, H. T.; Kim, S.; Yoon, S.; Kim, K. S.; Shin, J. S.; Suh, J. S.; *et al.* Nanoscale Size Effect of Magnetic Nanocrystals and Their Utilization for Cancer Diagnosis Via Magnetic Resonance Imaging. *J. Am. Chem. Soc.* **2005**, *127*, 5732–5733.
41. Turkevich, J.; Stevenson, P.; Hillier, J. A Study of the Nucleation and Growth Processes in Teh Synthesis of Colloidal Gold. *Discuss. Faraday Soc.* **1951**, *11*, 55–75.
42. Paik, T.; Ko, D. K.; Gordon, T. R.; Doan-Nguyen, V.; Murray, C. B. Studies of Liquid Crystalline Self-Assembly of GdF(3) Nanoplates by in-Plane, out-of-Plane SAXS. *ACS Nano* **2011**, *5*, 8322–8330.
43. Horak, D.; Babic, M.; Jendelova, P.; Herynek, V.; Trchova, M.; Pientka, Z.; Pollert, E.; Hajek, M.; Sykova, E. D-Mannose-Modified Iron Oxide Nanoparticles for Stem Cell Labeling. *Bioconjugate Chem.* **2007**, *18*, 635–644.